Methodology and Error Analysis of Direct Resistance Measurements Used for the Quantification of Boron–Hydrogen Pairs in Crystalline Silicon

Axel Herguth ⓘ, *Member, IEEE*, and Clemens Winter ⓘ

Abstract—A method for quantifying dopant–hydrogen pairs and their formation dynamics in crystalline silicon by means of directly contacted resistance measurements is presented and exemplarily validated. The method can also be applied in-situ in the temperature range where dopant–hydrogen pair formation occurs. Furthermore, the influence of different confounding factors such as a faulty assumption of doping level, unnoticed temperature variations, and unwanted illumination is quantified. It is concluded that the detection limit of dopant–hydrogen pairs of the presented method is most likely limited by unnoticed temperature fluctuations and scales with the actual dopant concentration. For crystalline silicon doped with 10^{16} cm^{-3} as it is usually used for photovoltaic applications, the detection limit is found to be below 10^{13} cm^{-3}.

Index Terms—Boron–hydrogen pairs, crystalline silicon (c-Si), hydrogen, measurement technique.

I. INTRODUCTION

HYDROGEN plays an important role in crystalline silicon (c-Si), because it can move comparatively easily, i.e., already at low temperature, and it tends to bind to impurities and structural defects (e.g., dangling bonds), thus changing their electronic structure [1]. Especially for recombination active structures (defects) featuring an energy state deep in the band gap of silicon, passivation by hydrogen can drastically lower the recombination activity observable in an increase in excess charge carrier lifetime. Therefore, hydrogenation of the silicon bulk (especially for structural compromised materials like multicrystalline silicon) [2] and its interfaces [3] is an essential process step for applications like silicon solar cells relying on sufficiently high excess charge carrier lifetimes [4].

The tendency of hydrogen to bind to impurities or structural defects gives rise to multifaceted reaction dynamics in parts reflected by dynamic changes of excess charge carrier lifetime. For instance, hydrogen is suspected to passivate the defect responsible for boron-oxygen-related light-induced degradation under certain circumstances [5], [6]. Hydrogen is suspected as well to be the driving force behind light- and elevated temperature-induced degradation [7], [8] and maybe behind the degradation of surface passivation as well [9].

Unfortunately, hydrogen is a rather hard-to-grab species in silicon because its equilibrium concentration is determined mainly by the concentration of impurities ready to bind it. This reaches so far that atomic (meaning unbound) hydrogen seems to be practically insoluble in virtually impurity- and dopant-free silicon [1].

Quantification of hydrogen (^{1}H) by means of secondary ion mass spectrometry is typically limited by residual gas contamination to the 10^{18} cm^{-3} range [10]. However, it can be improved considerably when deuterium (^{2}H) is intentionally used in experiments, improving the detection limit to the 10^{14} cm^{-3} range due to the ^{2}H/^{1}H natural isotope abundance ratio of $\sim 10^{-4}$.

For doped silicon, charged dopant atoms like boron (B$^-$; p-type) or phosphorous (P$^+$; n-type) are one of the major trapping sites for typically charged hydrogen (H$^+$, H$^-$) and, in consequence, dopant–hydrogen pairs like BH can form [11]–[13]. These dopant–hydrogen pairs can be detected, e.g., by infrared absorption spectroscopy (FTIR), however, the detection of small quantities in the 10^{15} cm^{-3} range typically requires a comparatively thick sample and cryogenic temperatures [13].

It is important to note that the formation of dopant–hydrogen pairs, e.g., via the reaction $2\,B^- + H_2 + 2\,h^+ \rightarrow 2\,BH^0$, negates the doping effect. This opens up a way to indirectly detect and quantify hydrogen by its effect on material conductivity σ or resistivity ρ, respectively.

In the past, this effect has been widely used to study BH dynamics by means of spreading resistance measurements [11], [14] and capacitive techniques [15]–[18], both capable of determining a depth-resolved dopant profile. This is especially important for in-diffusion experiments relying on the change of net dopant concentration profiles.

Recently, Walter *et al.* [19] successfully exploited the (depth-averaged) change in resistivity due to the formation of BH pairs by means of contact-free eddy-current measurements where the sample is placed on top of an induction coil integrated in a resonant circuit of a lifetime tester from Sinton Instruments [20]. In order to trigger boron–hydrogen formation dynamics, Walter

et al. [19] annealed the samples in the dark at elevated temperatures in alternation with manual ex-situ measurements at room temperature. Walter *et al.* [19] also demonstrated that the detection limit of hydrogen by means of BH pairs formation depends crucially on the uncertainty of the resistivity measurement.

Within this contribution, depth-averaged material resistivity ρ is measured by directly contacting the silicon substrate paving the way to a fully automated in-situ measurement of dopant–hydrogen pair formation dynamics while still allowing for lifetime measurements to track lifetime changes.

II. THEORETICAL BACKGROUND

A. Impact of Boron–Hydrogen Pairs on Resistivity

In the following, the focus shall lie on p-type material typically used for photovoltaics with a (net) dopant concentration N_{dop} in the range of 10^{15}–10^{16} cm^{-3}. Material conductivity σ or resistivity ρ

$$\sigma = \rho^{-1} = q \cdot (p \cdot \mu_p + n \cdot \mu_n) \tag{1}$$

depends on elementary charge q, total hole and electron concentrations p and n as well as on their respective mobilities μ_p and μ_n. It is noteworthy that these mobilities generally depend on total carrier concentrations as well as on temperature T as discussed later on and illustrated in Appendix A. In this article, mobilities are taken from [21], based on various models [22]–[26].

Total charge carrier concentrations p and n are defined as

$$p = p_0 + \Delta p \text{ and } n = n_0 + \Delta n \approx \Delta n \tag{2}$$

where p_0 and n_0 are hole and electron concentrations in thermal equilibrium (in darkness). Note that $n_0 = n_i^2 / p_0$, with n_i being the intrinsic charge carrier concentration is negligible compared to p_0 for p-type material (except for very low doping and high temperatures, see Appendix A). Excess charge carrier concentrations Δp and Δn can be introduced, e. g., by illuminating the sample where $\Delta p = \Delta n \gg n_0$ in the following. Especially unwanted illumination should be avoided as discussed later on.

At room temperature and above, dopant atoms are mostly activated, so that the equilibrium hole concentration p_0 is given by the background (acceptor) net doping concentration $N_{dop} \gg n_i$, which is probably close to but not necessarily identical with the boron concentration $[B]$. The latter is of course a prerequisite for BH pair formation. However, as introduced before, this pair formation neutralizes in parts the boron doping so that

$$p_0 = N_{dop} - [BH] \tag{3}$$

Hence, conductivity σ or resistivity ρ (and its change) is a direct measure of BH pair concentration $[BH]$

$$\sigma = \rho^{-1} = q \cdot \mu_p \cdot \left\{ N_{dop} - [BH] + \Delta n \cdot \left(1 + \frac{\mu_n}{\mu_p} \right) \right\} \tag{4}$$

and, depending on reaction conditions, a measure for hydrogen concentration itself [19], [27]. As measurements take place in darkness ($\Delta n \ll p_0$), the last term is considered only as a possible error source discussed later on.

B. Boron–Hydrogen Pair Formation Dynamics

As the focus of this article shall not lie on the exact description of BH pair formation dynamics, only a simple model is used here. A more detailed model has been presented elsewhere [19], [27], explicitly taking the dependences on hole concentrations into account.

Experimental data suggest that hydrogen released from dielectric layers during a high temperature firing step ($>650\,°C$) with a rapid cool-down phase predominantly forms hydrogen dimers denoted as H_{2A} [13], [27]. As this seems not to be the equilibrium state at low temperature and BH pairs seem more favorable, the hydrogen system relaxes following the reaction path $H_{2A} + 2\,B^- + 2\,h^+ \leftrightarrows 2\,BH^0$ [13], [27]. However, BH pairs do not seem to be the most favorable state because it is observed that these pairs vanish for longer times as well. It is speculated that hydrogen detaches and forms a different dimeric configuration denoted as H_{2C}, which seems to be more stable compared to H_{2A} [27]. Hence, for longer times the hydrogen system seems to follow the reaction $2\,BH \leftrightarrows H_{2C} + 2\,B^- + 2\,h^+$. If the supply with holes is considered constant over time, meaning $[BH] \ll N_{dop}$, the hydrogen system can be described by the set of differential equations

$$\frac{d}{dt} \begin{bmatrix} [H_{2A}] \\ [BH] \\ [H_{2C}] \end{bmatrix} = \begin{bmatrix} -\kappa_{12} & +\kappa_{21} & 0 \\ +\kappa_{12} & -(\kappa_{21} + \kappa_{23}) & +\kappa_{32} \\ 0 & +\kappa_{23} & -\kappa_{32} \end{bmatrix} \cdot \begin{bmatrix} [H_{2A}] \\ [BH] \\ [H_{2C}] \end{bmatrix}. \tag{5}$$

The time-dependent solution for $[BH]$ is given by a sum of exponential functions

$$[BH](t) = A_1 \cdot \exp(-t/t_1) + A_2 \cdot \exp(-t/t_2) + A_\infty \tag{6}$$

characterized by their respective time constants t_1 and t_2. The exact dependence of t_1 and t_2 on κ_{ij} is not of importance here and can be found elsewhere [28]. Hence, ignoring changes in mobility for the time being, the observable change in conductivity $\Delta\sigma$ with time

$$\Delta\sigma = \sigma(t = 0) - \sigma(t) \propto \Delta[BH] \tag{7}$$

is expected to follow such a curve. Using the difference also relaxes the need for an exact knowledge of the background doping N_{dop} and allows non-zero $[BH]$ at $t = 0$ as well.

It should be noted that all variations in measured resistivity (conductivity) are solely attributed to a change in $[BH]$. Therefore, this approach is not applicable to conditions known to impact background doping, e.g., thermal donor formation. Furthermore, it has to be ensured that other factors such as a changing contact resistance are not misinterpreted as BH pair related change.

III. SAMPLE DESIGN AND MEASUREMENT SETUP

The sample design illustrated in Fig. 1 was chosen to allow for both, contact-free excess charge carrier lifetime measurements via photoconductance decay (PCD) [20] with the above-mentioned lifetime tester from Sinton Instruments as well as directly contacted resistivity measurements.
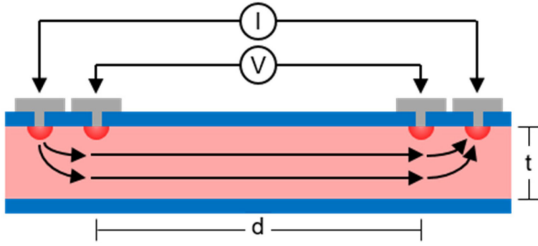
Fig. 1. Sketched sample and measurement design (not to scale). Two Al double stripe-shaped electrodes (gray) are deposited on top of the dielectric layer (blue) on opposite sides of the 5×5 cm c-Si sample (red). Pointwise heating by laser drives Al through the dielectric where it alloys with the silicon substrate (dark red semicircles) and thus forms an ohmic contact (LFC). Resistivity of the c-Si substrate is measured in a four-terminal configuration rejecting lead resistances and spreading resistance effects. Spacing between the inner electrodes is large enough to allow for PCD measurements as well.

The measurement of excess charge carrier lifetime requires a sample with both-sided passivated surfaces. In the following, this is done by depositing a hydrogen-rich silicon nitride (SiN_x:H) via plasma enhanced chemical vapor deposition in a PlasmaLab100 from Oxford Instruments, which acts as hydrogen source during a following high temperature firing step [3], [29]. Furthermore, the PCD measurement requires a metal-free area of ~ 35 mm in diameter [30], [31].

In order to obtain a reliable contact to the comparatively low doped silicon substrate, in our case boron-doped floatzone silicon (FZ-Si) with $\rho \sim 1$ $\Omega \cdot$cm ($p_0 \sim 1.5 \times 10^{16}$ cm^{-3}), through the SiN_x:H layer, aluminum is first deposited via thermal evaporation in a pattern of two stripe-shaped electrodes each on opposite sides of the 5×5 cm^2 sample. In a second step, a multitude of laser fired contacts (LFC) is formed [32], [33]. During the laser process, the aluminum penetrates the SiN_x:H layer and locally alloys with the silicon substrate, thus forming a strongly Al-doped (p$^+$) region underneath the LFC, which helps to establish a reliable low resistance contact to the otherwise weakly doped substrate. Even though a single LFC comes with a resistance of ~ 100 Ω, the multitude of LFCs reduces the contact resistance of a stripe to ~ 1 Ω (or below). In contrast, the resistance path within the substrate in between the inner electrodes with distance $d = 4$ cm comes for a sample with thickness $t = 250$ μm and width $w = 5$ cm with a resistance R

$$R = \rho \cdot \frac{g \cdot d}{w \cdot t} \tag{8}$$

of ~ 33 Ω for $\rho = 1$ $\Omega \cdot$cm material. As the contact resistance in the range of ~ 1 Ω would obviously cause a non-negligible error of several percent in a two-terminal measurement, a four-terminal configuration is chosen instead, using the outer opposing electrodes for current injection and extraction, and the inner stripes as voltage probes. This configuration virtually cancels the effect of contact resistance of the outer electrodes. As it is hard to align the LFCs in practice up to the very edge of the sample, a geometry coefficient $g \neq 1$ is introduced to compensate for the noncontacted edge region and the resulting inhomogeneous current distribution. A value of $g \sim 1.02$ is derived from

simulation for our sample design taking also the resistance contribution along the 60 nm thick Al stripes into account.

For the resistance measurements, a 6½-digit digital multimeter (type Keithley 2000) is used. As will be presented in the following, two setups were used: For ex-situ measurements at room temperature (25 °C) samples are placed on a water-cooled/heated sample mount in a light-tight housing. For in-situ measurements at elevated temperatures, the sample is placed on a hotplate (type Praezitherm PZ 28-2). Sample contacting was done with thin steel needles.

IV. Exemplary Measurements

A. Ex-Situ Measurements

Samples are dark annealed at elevated temperatures to allow the BH pairing reaction to take place in an experimentally accessible time scale. Samples are removed from the hotplate (Praezitherm PZ 28-2) periodically to measure the electrical resistance. Exemplary measurements of three identically processed FZ-Si samples ($\rho \sim 1.1$ $\Omega \cdot$cm) during either annealing in darkness at 180 °C or storage at room temperature (as reference) are displayed in Fig. 2 (top). Resistance rises with ongoing treatment time indicating BH pair formation and reaches a maximum after ~ 50 h followed by a decrease, which has not reached a saturation even after more than 2000 h. The sample stored at room temperature remains at its initial value for the entire period of time.

With (4) and (8), the change in resistance is converted to a change in BH pair density $\Delta[BH]$ shown in Fig. 2 (bottom). The rise and decline of resistance transfers directly to $\Delta[BH]$. Since only changes with respect to the starting value are considered in the calculation of $\Delta[BH]$, the measured offset in resistance between samples 1 and 2 vanishes almost entirely. Sample 3 is not expected to change over time. The small observed unsystematic scattering with a standard deviation of 7×10^{12} cm^{-3} is most likely a measure of temperature variations in our configuration (Section V-G) and demonstrates the excellent stability of the room temperature setup also for an extended time period of three month (2200 h).

One unavoidable issue with the ex-situ setup is that the thermal equilibrium of the setup is disturbed each time a sample is inserted. Hence, the result of a single measurement depends to some extent on how long the setup and sample are allowed to equilibrate before the measurement. Fig. 3 shows the result of a measurement series where the sample was intentionally not removed for an extended period of time. As can be seen, fluctuations in $\Delta[BH]$ are noticably smaller then and even the impact of room temperature variations in form of day-night cycles can be resolved. The superimposed linear drift might be the beginning of BH pair formation strongly slowed down due to the low temperature compared to Fig. 2.

The excellent agreement of the theoretically predicted BH pairing and dissociation dynamic (6) with measurement data as shown in Fig. 2 (bottom) validates the simplified model. For very long treatment times >3000 h a negative value of $\Delta[BH]$ is predicted by the fits. This is in agreement with observations that after introducing hydrogen into the silicon bulk with a high
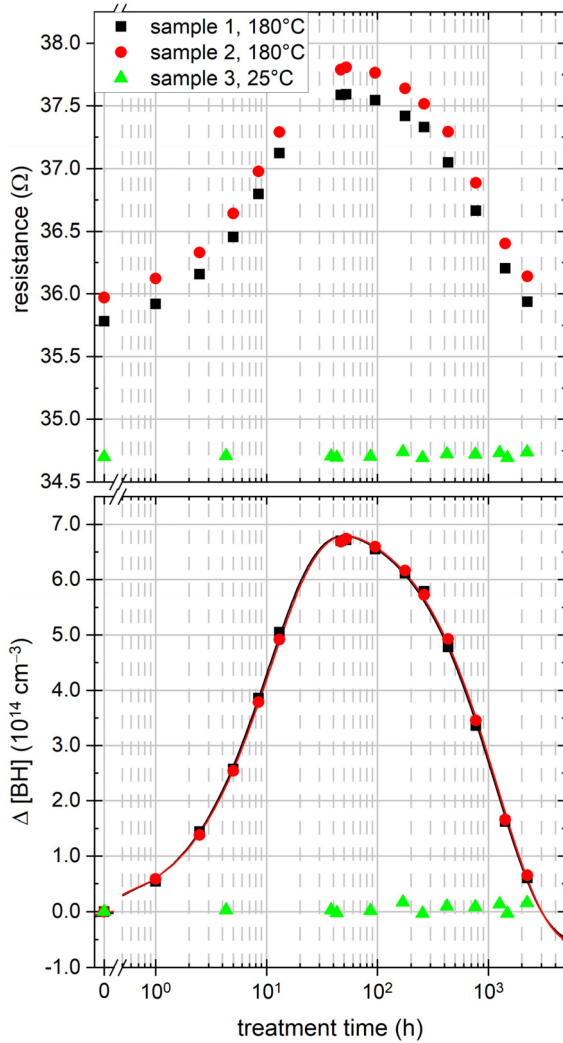
Fig. 2. (Top) Development of measured electrical resistance during annealing in the darkness of three identically processed samples at 180 °C and room temperature, respectively. (bottom) Calculated change in BH-pair concentration $\Delta[BH]$. Lines are fits according to (6).

temperature step followed by a rapid cooldown, there exists an initial concentration of BH pairs $[BH](t = 0) > 0$ [12], [13].

B. In-Situ Measurements

All measurements presented so far were done by manually removing the sample from the hotplate, transferring it to the measurement setup in a light-tight box, contacting the sample with the test probes, performing the measurement, and placing it back on the hotplate. This handling takes time, implies the chance of damaging the sample and exposes it to uncontrolled temperature ramps and short intervals of ambient light exposure. A way to avoid these difficulties is by contacting the sample directly on the hotplate (in-situ). The use of a signal switchboard allows for the automated finely time-resolved resistance monitoring even of a multitude of samples in parallel. In addition, temperature can be tracked via a PT 100 sensor as well. An exemplary evolution of $\Delta[BH]$ measured in-situ with an interval of 10 s is
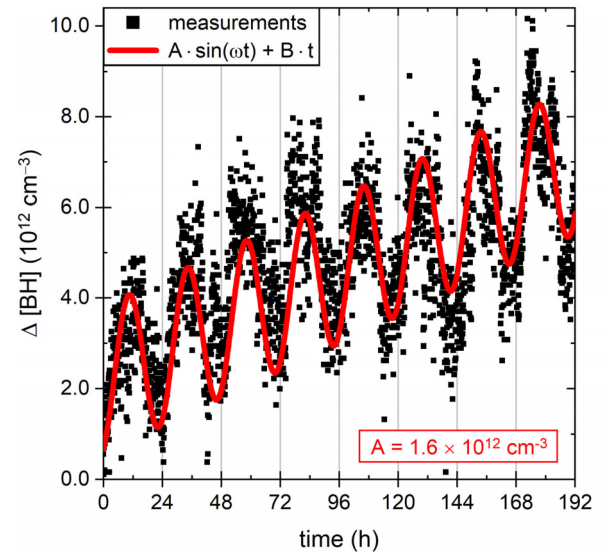

Fig. 3. Measurement series with a sample permanently left in the ex-situ setup which is stabilized to 25 °C by water cooling/heating. The oscillation period of 24 h suggests a 24-h day-night cycle.
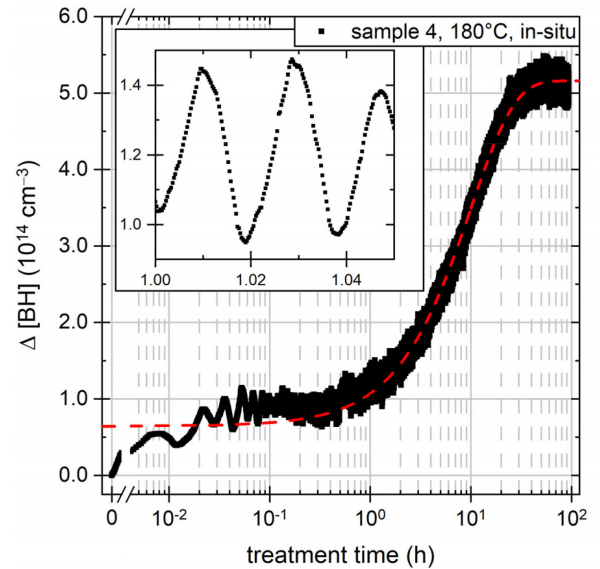

Fig. 4. In-situ measurement of a sample treated at 180 °C, with a sampling rate of 10 s. Short-term oscillations can be attributed to small periodical changes in temperature which directly affect the hole mobility and thus cause an apparent change in BH pair density $\Delta[BH]$. The dashed line is a fit according to (6) with A_2 fixed to zero.

displayed in Fig. 4. The maximum BH pair density is reached in a similar time scale as with the ex-situ measurement showing that interrupting the dark anneal regularly does not significantly change the fundamental behavior. The short-term oscillations visible in Fig. 4 can be attributed to small periodical changes in the hotplate temperature as a result of regulation by heating and cooling. As will be discussed later on, temperature changes not explicitly considered during conversion of resistance to BH pair density result in an apparent change in $\Delta[BH]$ as discussed in Section V-C.

V. EXPECTABLE ACCURACY

To optimize the accuracy of the described method, it is important to understand the different sources of error and to distinguish between general errors and errors resulting from deviations between measurements.

As the error of different influencing factors is not independent of each other, their individual impact is first estimated in the following Sections V-A–V-E. In Section V-F, a Monte-Carlo simulation is used to exemplarily demonstrate the impact of error in different scenarios. Section V-G addresses the expectable detection limit of $\Delta[BH]$.

For a perfectly dark experiment, where Δn can be neglected, the BH pair density $[BH]$ follows from (4) and (8)

$$[BH] = N_{dop} - f_g \cdot \frac{1}{\mu_p \cdot R} \text{ with } f_g = \frac{g \cdot d}{q \cdot w \cdot t}. \quad (9)$$

An erroneous assumption for the background net dopant density N_{dop} leads to an offset in total BH pair density. Taking the difference between measurements $B(efore)$ and $A(fter)$ a treatment step, thus calculating the change in BH pairs density $\Delta[BH]$

$$\Delta[BH] = f_g \cdot \left(\frac{1}{\mu_{p,B} \cdot R_B} - \frac{1}{\mu_{p,A} \cdot R_A} \right) \quad (10)$$

eliminates this offset, however, only under the assumption that the treatment step does not change the background doping.

While f_g comprises only geometrical information that will probably not change in between measurements, the second bracketed factor is expected to change.

A. Resistance Measurement Related Errors

Test measurements in the 4-terminal resistance configuration with the 6½-digit digital multimeter used in our experiments revealed a relative accuracy $\delta R/R$ of 1.6×10^{-3} %. Hence we conclude that the resistance measurement itself does neither contribute significantly to the resistance measurement of the sample nor temperature measurement with the resistance thermometer (type PT 100). Hence, one could even use a less accurate resistance measurement setup.

B. Sample Geometry Related Errors

From (10) it follows that the relative error of $\Delta[BH]$ may be approximated by the law of error propagation for independent relative errors of the geometrical parameters

$$\frac{\delta \Delta[BH]}{\Delta[BH]} = \frac{\delta f_g}{f_g} = \left\{ \left(\frac{\delta g}{g} \right)^2 + \left(\frac{\delta d}{d} \right)^2 \right.$$
$$\left. + \left(\frac{\delta w}{w} \right)^2 + \left(\frac{\delta t}{t} \right)^2 \right\}^{1/2}. \quad (11)$$

Thus, a relative error in geometrical information directly translates to a relative error of $\Delta[BH]$. If, for example, a relative error below 1% for $\Delta[BH]$ is desirable, the geometric information needs to be sufficiently exact. For the samples used in the experiments, it implies a maximal error of δd of
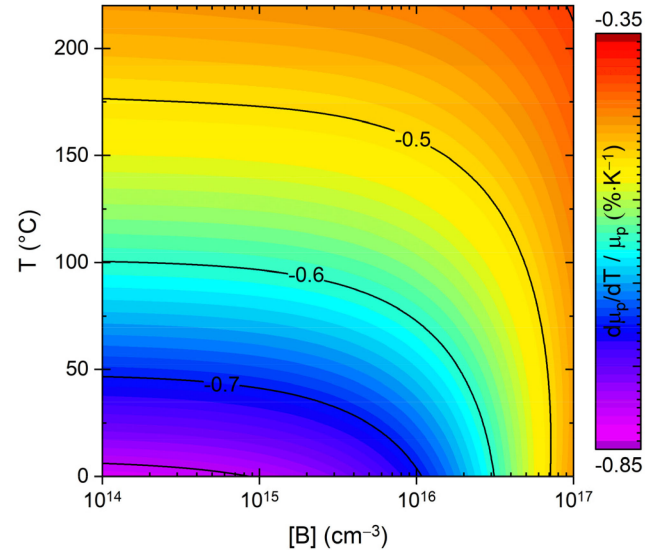

Fig. 5. Relative change in hole mobility μ_p with temperature T. Based on data from [21].

400 μm for an electrode distance d of 4 cm or δw of 500 μm for a sample width w of 5 cm or δt of 2.5 μm for a sample thickness t of 250 μm. The relative error of g is harder to assess because it comprises sample-specific information such as the exact electrode positioning. Neglecting the deviation of $\sim$2% from unity in the used configuration would accordingly imply 2% relative error of $\Delta[BH]$.

Errors in sample geometry imply subsequent errors in hole concentration and mobility which are discussed later on.

It should be noted that (7) and (10) do not cover the case of inhomogeneous sample geometry, e.g., a wedge-shaped sample with a thickness gradient across the sample. The effect of inhomogeneous thickness is addressed in Appendix B.

C. Temperature-Related Errors

Hole mobility μ_p in (10) depends quite strongly on temperature T as shown in Appendix A. Linear error propagation suggests

$$\delta \Delta[BH] = \frac{\partial \Delta[BH]}{\partial \mu_B} \cdot \frac{\partial \mu_B}{\partial T} \cdot \delta T_B + \frac{\partial \Delta[BH]}{\partial \mu_A} \cdot \frac{\partial \mu_A}{\partial T} \cdot \delta T_A \quad (12)$$

and finally yields

$$\delta \Delta[BH] = p_{0,A} \cdot \frac{\frac{\partial \mu_{p,A}}{\partial T}}{\mu_{p,A}} \cdot \delta T_A - p_{0,B} \cdot \frac{\frac{\partial \mu_{p,B}}{\partial T}}{\mu_{p,B}} \cdot \delta T_B. \quad (13)$$

Thus, temperature-related error is proportional to the hole concentration and the relative change in hole mobility with temperature. The latter is exemplarily depicted in Fig. 5 for a large range of boron concentrations $[B]$ and temperatures T. In our experiment with $p_0 = 1.5 \times 10^{16}$ cm^{-3} and $T = 25$ °C, relative change in hole mobility is -0.64 %·K^{-1}. Thus, ignoring an (unnoticed) increase in temperature of 0.1 °C between the measurements causes an apparent $\Delta[BH]$ gain of $\sim 1 \times 10^{13}$ cm^{-3}. The observed standard deviation of 7×10^{12} cm^{-3} for

This article has been accepted for inclusion in a future issue of this journal. Content is final as presented, with the exception of pagination.

6   IEEE JOURNAL OF PHOTOVOLTAICS

the green data in Fig. 2 implies a temperature variation δT of ± 75 mK for our ex-situ room temperature setup when samples are inserted and removed for each measurement. The even smaller deviation in Fig. 3 suggests that temperature variation may be even better when the setup and sample are granted the time to thermally equilibrate.

The measurement of $\Delta[BH]$ generally gets less sensitive to temperature errors with increasing temperature. For example, at an elevated temperature of 180 °C, the relative change in hole mobility is noticeably reduced to $-0.48\% \cdot \text{K}^{-1}$. However, the hotplate used in our in-situ setup for elevated temperatures is more prone to temperature variations than the water-cooled system used for ex-situ measurements at room temperature. In fact, temperature variations are the driving force behind the observed oscillations in Fig. 4. The appropriate countermeasure is temperature monitoring that allows for a compensation of temperature-related errors and plays an important role for the detection limit of $\Delta[BH]$ as discussed in Section V-G.

A systematic offset in both, δT_B and δT_A, cancels out for the most part. However, a (p_0-induced) difference in mobility and its change with temperature leads to a residual error as shown in Section V-F.

D. Hole Concentration Related Errors

Hole mobility μ_p depends on the total hole concentration p_0 as well. Unlike the geometrical information that contributes only to the pre-factor in (10), hole mobility is explicitly expected to change due to a changing hole concentration and thus the $\Delta[BH]$ error depends on the individual errors of mobility in both measurements.

As the impact of the relative error/deviation of the used/measured p_0 value from its true value p_{ref}, thus $\delta p_0 / p_{\text{ref}}$, is of interest, we switch to the dependence of hole mobility on the normalized hole concentration $\tilde{p}_0 = p_0 / p_{\text{ref}}$, thus $\mu_p(\tilde{p})$. In the ideal case, the used p_0 value is identical with the true value p_{ref}, thus $\tilde{p}_0 = 1$. Error propagation then suggests

$$\delta \Delta[BH] = \frac{\partial \Delta[BH]}{\partial \mu_{p,B}} \cdot \frac{\partial \mu_{p,B}}{\partial \tilde{p}_{0,B}} \cdot \delta \tilde{p}_{0,B}$$
$$+ \frac{\partial \Delta[BH]}{\partial \mu_{p,A}} \cdot \frac{\partial \mu_{p,A}}{\partial \tilde{p}_{0,A}} \cdot \delta \tilde{p}_{0,A} \qquad (14)$$

and finally yields

$$\delta \Delta[BH] = p_{0,A} \cdot \frac{\frac{\partial \mu_{p,A}}{\partial \tilde{p}_{0,A}}}{\mu_{p,A}} \cdot \delta \tilde{p}_{0,A} - p_{0,B} \cdot \frac{\frac{\partial \mu_{p,B}}{\partial \tilde{p}_{0,B}}}{\mu_{p,B}} \cdot \delta \tilde{p}_{0,B}. \qquad (15)$$

Thus, hole concentration related error is proportional to the hole concentration and the relative change in hole mobility with hole concentration. The latter is exemplarily depicted in Fig. 6 for a large range of boron concentrations $[B]$ and temperatures T. In our experiment with $p_0 = 1.5 \times 10^{16}$ cm^{-3} and $T = 25$ °C, relative change in hole mobility is $-0.8‰$ per % change in hole concentration. Thus, ignoring an (unnoticed) decrease of hole concentration of 1% between the measurements causes an apparent $\Delta[BH]$ loss of $\sim 1 \times 10^{13}$ cm^{-3}. The sensitivity towards errors in p_0 reduces with increasing temperature as well.
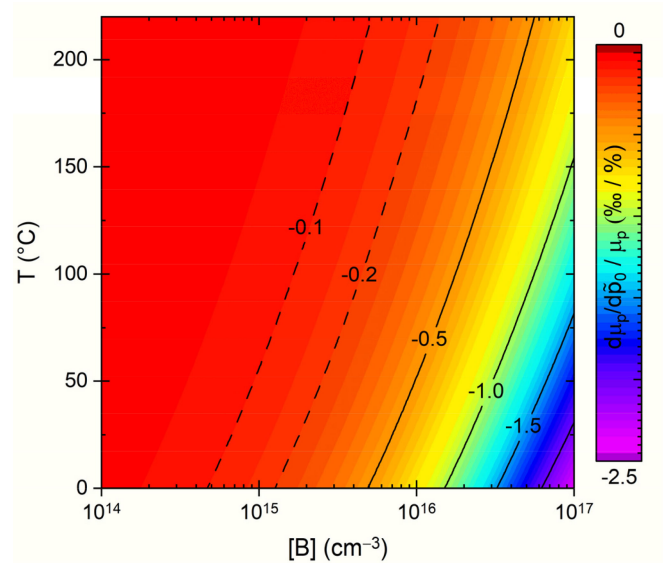

Fig. 6.   Relative change in hole mobility μ_p with normalized hole concentration. Based on data from [21].

Note that due to the subtraction, a systematic offset error in p_0 cancels out to some extent.

It is especially important to take the change in p_0 and thus μ_p in between the measurements into account. Calculating, for example, with an unchanged hole mobility $\mu_B = \mu_A$, even though BH pair formation results in $p_{0,B} > p_{0,A}$, leads to a systematic underestimation of $\Delta[BH]$ as demonstrated in Section V-F.

To avoid that problem, hole concentration and mobility should be determined self-consistently for each measurement from the measured resistance R according to the equation

$$p_0 \cdot \mu_p = f_g \cdot \frac{1}{R}. \qquad (16)$$

An error in geometrical information implies an error in the product as well. However, considering the weak relative change of hole mobility with hole concentration virtually the whole relative error of the geometrical information goes to the relative error of hole concentration. Hence a cumulative relative error of 1% in geometrical information yields almost 1% error in p_0, which then contributes to an additional p_0 related error of $\Delta[BH]$.

E. Injection-Related Errors

If the measurement does not take place in perfect darkness, illumination generates excess charge carriers that might be mistaken as BH pairs. The absolute density of these false BH pairs scales with injection Δn, or better the difference between measurements $B(efore)$ and $A(fter)$ a treatment step

$$\Delta[BH] = \Delta[BH]_{dark} + (\Delta n_B - \Delta n_A)\left(1 + \frac{\mu_n}{\mu_p}\right). \qquad (17)$$

The last factor comprises the ratio of electron and hole mobility, which is almost constant in the range of 2.5 at 25 °C. Thus the last factor contributes in total a factor of 3.5. Hence, a difference
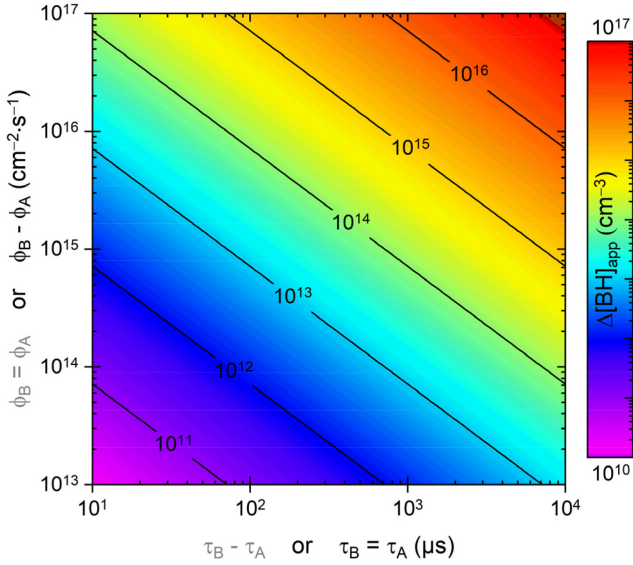
Fig. 7. Apparent BH pair density $\Delta[BH]_{app}$ related either to changing lifetime $\tau_B - \tau_A$ with fixed photon flux $\phi_B = \phi_A$ or changing photon flux $\phi_B - \phi_A$ with fixed lifetime $\tau_B = \tau_A$. For negative differences (not shown) $\Delta[BH]_{app}$ turns negative as well.
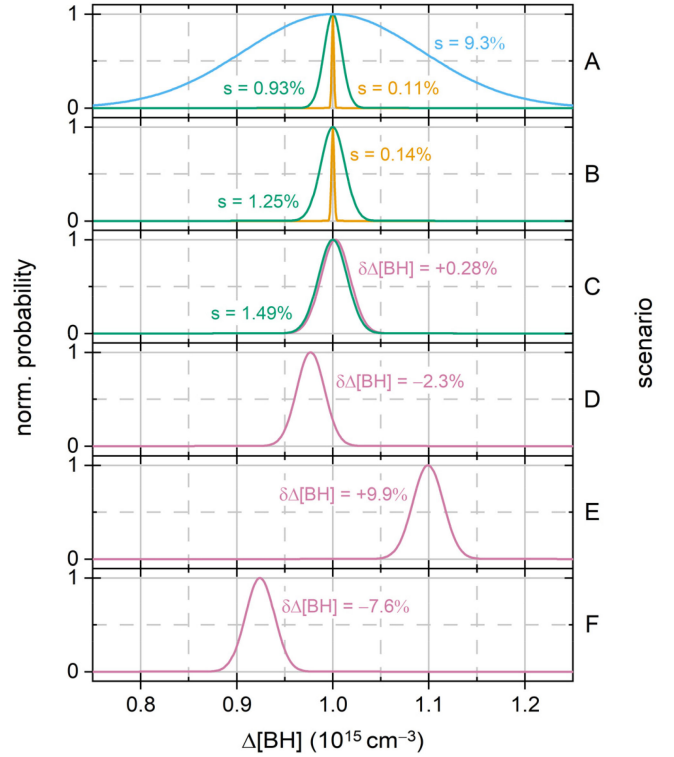

Fig. 8. Distribution of $\Delta[BH]$ from Monte-Carlo simulations for different scenarios with $[B] = 1.5 \times 10^{16}$ cm^{-3} and $[BH]$ increasing from 0 cm^{-3} before to 10^{15} cm^{-3} after a treatment step.

in injection of $\sim 3 \times 10^{13}$ cm^{-3} between the measurements results in an apparent gain or loss of $\sim 1 \times 10^{14}$ cm^{-3} BH pairs.

Obtained injection Δn scales on the one hand with the (re-flection corrected) photon flux ϕ absorbed in the sample and effective excess charge carrier lifetime τ. Assuming a perfect redistribution of actually inhomogeneously generated excess charge carriers over the total sample thickness t, injection Δn can be estimated as

$$\Delta n = \frac{\phi}{t} \cdot \tau. \qquad (18)$$

Thus injection related apparent change in BH pair density $\Delta[BH]_{app}$ scales with

$$\Delta[BH]_{app} = \frac{1}{t} \cdot \left(1 + \frac{\mu_n}{\mu_p}\right) \cdot (\phi_B \cdot \tau_B - \phi_A \cdot \tau_A). \qquad (19)$$

The impact of changing photon flux or changing lifetime is illustrated in Fig. 7. For comparison, the photon flux of "1 sun" [34] is of the order of 10^{17} cm$^2 \cdot$s^{-1}. Artificial lighting typically ranges between 10^{14} (1 ‰ sun) and 10^{15} cm$^2 \cdot$s^{-1} (1 % sun).

If for example, a sample with constant lifetime $\tau = 10^3$ µs (a value easily achievable for a sample with reasonable surface pas-sivation) is measured before a treatment step with room lighting switched ON and afterward switched OFF, thus that $\phi_B - \phi_A \sim$ 1 % sun, an additional $\Delta[BH]_{app}$ of $\sim 10^{14}$ cm^{-3} seems to be present in the sample. In comparison with the observed overall change in Fig. 2, this would have a non-negligible impact on the experiment.

In this context, it is also noteworthy that hydrogen dynamics are associated with defect formation inducing lifetime changes. For example, it may occur that lifetime drops from $\tau_B = 1000$ µs to $\tau_A = 100$ µs. Measuring with the room lighting of $\phi \sim$

1% sun switched ON, this lifetime drop implies a $\Delta[BH]_{app}$ of $\sim 10^{14}$ cm^{-3}; again a reasonable source of error.

Hence, it is highly advisable to carry out the resistance mea-surements in darkness to mostly eliminate this source of error.

F. Combined Errors in Monte-Carlo Simulations

The effect of various errors or their combination was studied by means of Monte-Carlo simulations. A multitude of 10^6 virtual experiments was performed and evaluated. Within each virtual experiment, each quantity was randomized within a certain error band assuming a uniform distribution. The resulting $\Delta[BH]$ histograms were found to be describable by a normal distribution characterized by its standard deviation s and in certain cases by deviation $\delta\Delta[BH]$ of its center from the known $\Delta[BH]$ input. Note that $\pm 2s$ cover $\sim 95\%$ of the results. The results for the base scenario of $[B] = 1.5 \times 10^{16}$ cm^{-3} and $[BH]$ increasing from 0 to 10^{15} cm^{-3} evaluated at 25 °C are shown in Fig. 8.

In *scenario A*, error in temperature δT_x is varied from 0.01 to 0.1 to 1 °C while neglecting geometrical errors. The width mostly corresponds to the estimation in Section V-C and demon-strates the need for appropriate temperature monitoring. In *sce-nario B*, each geometrical quantity is considered erroneous to 1‰ and 1%, respectively. Note that in this case, the width of the curve is not determined by differences in between measure-ments, but by deviations from the true values. The green curve in *scenario C* demonstrates the broadening due to the superposition of a 1% error in each geometrical quantity and a temperature

error of $\delta T_x = 0.1$ °C. The red curve illustrates the case that both measurements were erroneously performed at $26 \pm \delta T_x$°C, but evaluation takes place at 25 °C. The difference calculation in (10) eliminates most but not all of that error and leads to a small $\delta \Delta[BH]$ shift. *Scenario D* demonstrates the effect of ignoring the geometrical correction factor g, thus assuming $g = 1$ even though its true value is 1.02. The resulting shift of more than 2% is caused by an erroneous determination of p_0. *Scenario E* demonstrates the effect of an unnoticed temperature increase from 25 to 26 °C in between measurements as mentioned in Section V-C. *Scenario F* illustrates the effect of ignoring the p_0-induced change in mobility due to the formation of BH pairs, thus erroneously assuming $\mu_{p,B} = \mu_{p,A}$.

G. Detection Limit

As discussed above, errors in temperature are probably the most relevant error source for $\Delta[BH]$. Temperature is typically stabilized by (active) heating below a certain set temperature and (passive) cooling above it. Hence temperature is often found to oscillate with an amplitude δT around an average (set) value $\tilde{T}$ on a time scale typically by far longer than a single resistance measurement takes. Hence, averaging measurements taken in a few seconds do not reflect long-term oscillations in temperature as can be seen from Figs. 3 and 4 as well. If two measurements are longer apart in time, it is highly unlikely that both measurements are done at exactly the average temperature $\tilde{T}$ at which (10) is evaluated. In the worst case, actual temperatures $T_B = \tilde{T} + \delta T$ and $T_A = \tilde{T} - \delta T$ might differ by $2\delta T$ implying a temperature-induced change in mobility that might be misinterpreted as an apparent change in BH pair density $\Delta[BH]$ (see Section V-C). Thus, the true change in BH pair density must at least surpass that temperature-induced apparent change to be unambiguously interpreted as related to BH pair formation. This detection threshold can be estimated from (13) for the above-mentioned extreme case. A more thorough treatment yields

$$\Delta[BH] \geq -p_0 \cdot \sum_{n=1}^{\infty} 2 \cdot \left(\frac{\partial \mu_p / \partial T}{\mu_p} \cdot \delta T \right)^n \qquad (20)$$

in which the $n = 1$ term [corresponding to (13)] is already a good approximation of the quickly converging series with respect to the small relative change of mobility with temperature as shown in Fig. 5. Following the example from above, the material with $p_0 = 1.5 \times 10^{16}$ cm^{-3} used in the experiments features a relative change in mobility of -0.64 %·K^{-1} at 25 °C. The room temperature setup without explicit temperature monitoring is expected to be accurate to $\delta T = \pm 0.1$ °C (if not even better, if properly equilibrated; see Fig. 3), hence the detection limit of $\Delta[BH]$ should be in the range of 0.13 %·$p_0 \sim 2 \times 10^{13}$ cm^{-3}. A further reduction of the detection limit requires either a temperature monitoring or measurement spread over longer times to take long-term oscillations into account.

The lower relative change in mobility at elevated temperatures decreases the detection limit of $\Delta[BH]$, however, from experience, it is harder to stabilize the temperature of a hotplate than that of a water-cooled/heated setup. Hence, temperature monitoring is more relevant for (in-situ) measurements at elevated temperatures.

More generally speaking, the relative change in mobility (see Fig. 5) varies only weakly across the whole shown doping and temperature range and thus it seems fair to estimate the detection limit as a fixed fraction ~ 1 %·K$^{-1} \times \delta T$ of the doping level p_0.

VI. CONCLUSION

Resistivity changes related to the formation and dissociation of boron–hydrogen pairs can be reliably determined with high precision in directly contacted samples. For the calculation of BH pair densities, it is important to take mobility changes related to changing hole concentration and temperature into account. Especially unnoticed temperature variations are found to be the main limiting factor for measurement accuracy. In consequence, the detection limit of BH pairs in silicon is decisively determined by the quality of temperature control or monitoring.

Exemplary measurements confirm the (simplified) formation and dissociation theory. Due to a better temperature control, measurements with the room temperature *ex-situ* setup show superior results compared to the measurements done *in-situ* on a hotplate (without temperature monitoring). If setup and sample are granted the time to thermally equilibrate, even changes in BH pair concentrations in the low 10^{12} cm^{-3} range can be detected in silicon usually used for photovoltaic applications.

APPENDIX

A. Review of Doping and Temperature Dependence

Figs. 9–11 illustrate the changes in resistivity, hole concentration, and mobility of boron-doped silicon in a large range of doping concentrations and temperatures. In general, interactions of charged dopant atoms with charge carriers and of charge carriers among themselves imply a decrease of hole mobility with increasing dopant/hole concentration and increasing temperature. In addition, phonon scattering decreases mobility with increasing temperature as well. Resistivity reflects in large parts the changes in mobility because more or less all dopant atoms are already ionized in the shown temperature and doping range. A residual ionization effect is in theory still present for highly doped material ($>2 \times 10^{16}$ cm^{-3}) where p_0 increases slightly with temperature.

However, it should be noted that thermally driven band-to-band (intrinsic) excitation occurs as well. For lowly doped silicon (10^{14} cm^{-3}), thermally excited charge carrier concentration actually dominates over doping at elevated temperatures (>150 °C) causing the shown increase in p_0 and decrease in resistivity. In this case, the total hole concentration p_0 corresponds to the sum of holes introduced by the dopant density N_{dop} (completely activated) and thermally excited hole and electron concentrations $p_{0t} = n_{0t}$. Hence, conductivity σ or resistivity ρ follows from

$$\sigma = \rho^{-1} = q \cdot \mu_p \cdot \left\{ N_{dop} - [BH] + p_{0t} \cdot \left(1 + \frac{\mu_n}{\mu_p} \right) \right\} \qquad (21)$$
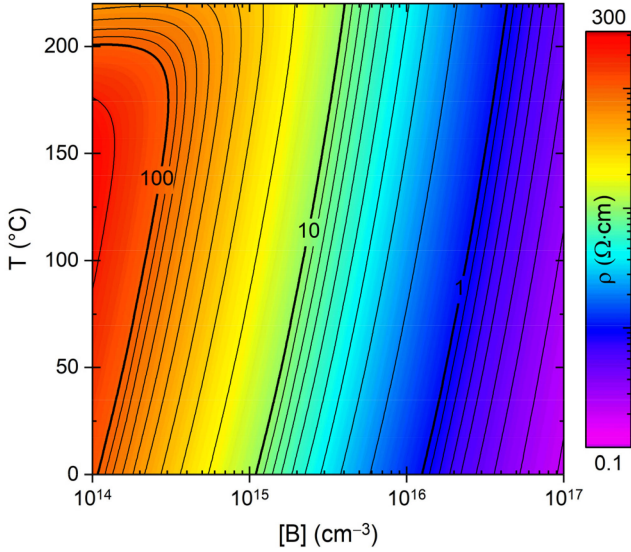
Fig. 9.   Resistivity ρ of boron-doped silicon in dependence of doping concentration $[B]$ and temperature T. Data from [21].
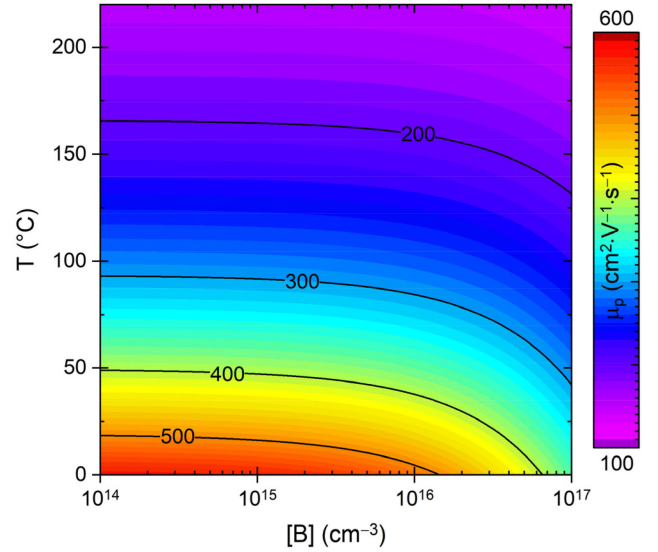

Fig. 11.   Hole mobility μ_p in boron-doped silicon in dependence of doping concentration $[B]$ and temperature T. Data from [21].
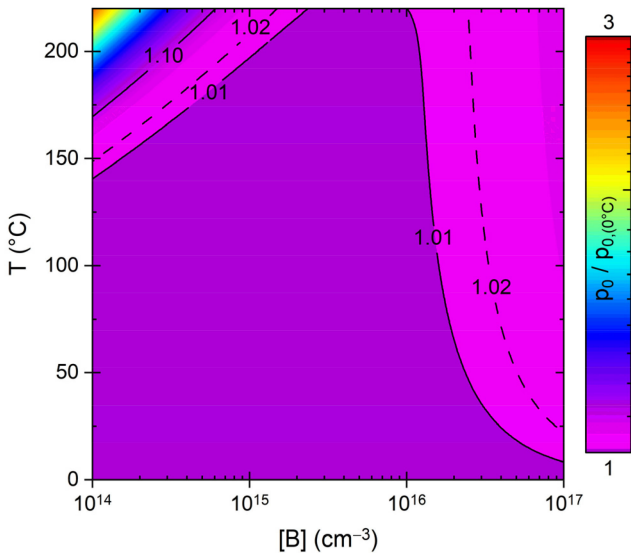

Fig. 10.   Hole concentration p_0 in boron-doped silicon in dependence of doping concentration $[B]$ and temperature T. Data from [21].

detection limit do not apply for lowly doped material at elevated temperatures.

B. Impact of Varying Sample Thickness

While the lateral sample dimensions (width w and electrode distance d) can be adjusted in the experiment, thickness t is probably harder to control and it cannot be excluded that thickness varies across the sample. Hence, calculation of resistivity from measured resistance might not always follow the ideal scenario described with (8).

For a wedge-shaped sample, for example, where thickness t

$$t\left(x\right) = t_0 \cdot \left(1 + \frac{\Delta t}{t_0} \cdot \frac{2}{d} \cdot x\right) \tag{23}$$

varies by $\pm\Delta t$ from average thickness t_0 in between the electrodes ($x = \pm d/2$), resistance R

$$R = \rho \cdot \frac{g \cdot d}{w \cdot t_0} \cdot \ln\left(\frac{1 + \Delta t/t_0}{1 - \Delta t/t_0}\right) / \left(2\frac{\Delta t}{t_0}\right) \tag{24}$$

deviates from the ideal scenario (8) by the latter term (which might be included in g as well). For example, a relative change in thickness of 10 % (thus in our case 250 ± 25 μm) yields a deviation in R of only $+3$ ‰. However, in our case, a thickness variation of 1% is more realistic.

The main reason for the comparatively small deviation is that the influence of thick and thin regions almost cancels out, but not completely because resistance scales inversely with thickness. Hence, using a laterally averaged thickness eliminates a thickness-related error in large parts.

which is more or less the same equation as (4) with thermal excitation instead of optical generation. Note that excited electrons do contribute more to conductivity due to their higher mobility ($\mu_n > \mu_p$). In principle, taking the difference

$$\Delta\sigma = \sigma_B - \sigma_A \propto \Delta\left[BH\right] \tag{22}$$

eliminates the influence of the thermally excited charge carriers and the above-described evaluation procedure remains valid. However, deviations in temperature in between the measurements are by far more critical because not only the comparatively weak change in mobility with temperature but also the strong change in p_{0t} with temperature plays a role. Hence, the aforementioned considerations for temperature-related errors and the

References

[1] S. J. Pearton, J. W. Corbett, and M. Stavola, *Hydrogen in Crystalline Semiconductors (Springer Series in Materials Science)*, vol. 16. Heidelberg, Germany: Springer, 1992.

[2] B. J. Hallam, P. G. Hamer *et al.*, "Development of advanced hydrogenation processes for silicon solar cells via an improved understanding of the behaviour of hydrogen in silicon," *Prog. Photovolt.: Res. Appl.*, vol. 28, no. 1, pp. 1217–1238, 2020, doi: 10.1002/pip.3240.

[3] R. S. Bonilla, B. Hoex, P. Hamer, and P. R. Wilshaw, "Dielectric surface passivation for silicon solar cells: A review," *Physica Status Solidi A*, vol. 214, no. 1-2, 2017, Art. no. 1700293, doi: 10.1002/pssa.201700293.

[4] B. Hallam *et al.*, "The role of hydrogenation and gettering in enhancing the efficiency of next-generation Si solar cells: An industrial perspective," *Physica Status Solidi A*, vol. 214, Jun. 2017, Art. no. 1700305, doi: 10.1002/pssa.201700305.

[5] T. Niewelt, J. Schön, W. Warta, S. Glunz, and M. Schubert, "Degradation of crystalline silicon due to boron-oxygen defects," *IEEE J. Photovolt.*, vol. 7, no. 1, pp. 383–398, Jan. 2017.

[6] A. Herguth and B. Hallam, "A generalized model for boron-oxygen related light-induced degradation in crystalline silicon," *AIP Conf. Proc.*, vol. 1999, 2018, Art. no. 130006, doi: 10.1063/1.5049325.

[7] J. Schmidt, D. Bredemeier, and D. C. Walter, "On the defect physics behind light and elevated temperature-induced degradation (LeTID) of multicrystalline silicon solar cells," *IEEE J. Photovolt.*, vol. 9, no. 6, pp. 1497–1503, Nov. 2019.

[8] D. Chen *et al.*, "Hydrogen-induced degradation: Explaining the mechanism behind light-and elevated temperature-induced degradation in n- and p-type silicon," *Sol. Energy Mater. Sol. Cells*, vol. 207, Apr. 2020, Art. no. 110353. 10.1016/j.solmat.2019.110353.

[9] D. Sperber, A. Graf, D. Skorka, A. Herguth, and G. Hahn, "Degradation of surface passivation on crystalline silicon and its impact on light-induced degradation experiments," *IEEE J. Photovolt.*, vol. 7, no. 6, pp. 1627–1634, Nov. 2017.

[10] F. A. Stevie *et al.*, "SIMS measurement of hydrogen and deuterium detection limits in silicon: Comparison of different SIMS instrumentation," *J. Vac. Sci. Technol. B*, vol. 34, no. 3, May. 2016, Art. no. 03H103, doi: 10.1116/1.4940151.

[11] J. I. Pankove, R. O. Wance, and J. E. Berkeyheiser, "Neutralization of acceptors in silicon by atomic hydrogen," *Appl. Phys. Lett.*, vol. 45, pp. 1100–1102, 1984, doi: 10.1063/1.95030.

[12] S. A. McQuaid, M. J. Binns, R. C. Newman, E. C. Lightowlers, and J. B. Clegg, "Solubility of hydrogen in silicon at 1300 °C," *Appl. Phys. Lett.*, vol. 62, no. 14, pp. 1612–1614, 1993, doi: 10.1063/1.108602.

[13] R. E. Pritchard, J. H. Tucker, R. C. Newman, and E. C. Lightowlers, "Hydrogen molecules in boron-doped crystalline silicon," *Semicond. Sci. Technol.*, vol. 14, no. 1, pp. 77–80, 1999, doi: 10.1088/0268-1242/14/1/011.

[14] M. W. Horn, J. M. Heddleson, and S. J. Fonash, "Permeation of hydrogen into silicon during low-energy hydrogen ion beam bombardment," *Appl. Phys. Lett.*, vol. 51, no. 7, pp. 490–492, 1987, doi: 10.1063/1.98376.

[15] C. H. Saeger and R. A. Anderson, "Real-time observations of hydrogen drift and diffusion in silicon," *Appl. Phys. Lett.*, vol. 53, no. 13, pp. 1181–1183, 1988, doi: 10.1063/1.100015.

[16] T. Zundel, A. Mesli, J. C. Muller, and P. Siffert, "Boron neutralization and hydrogen diffusion in silicon subjected to low-energy hydrogen implantation," *Appl. Phys. A*, vol. 48, pp. 31–40, 1989, doi: 10.1007/bf00617761.

[17] R. Rizk, P. de Mierry, D. Ballutaud, M. Aucouturier, and D. Mathiot, "Hydrogen diffusion and passivation processes in p- and n-type crystalline silicon," *Phys. Rev. B*, vol. 44, pp. 6141–6151, Sep. 1991, doi: 10.1103/physrevb.44.6141.

[18] E. M. Filangeri and T. Nishida, "Hydrogenation of boron in silicon during low temperature gas and liquid phase processing," *J. Appl. Phys.*, vol. 76, no. 1, pp. 332–335, 1994, doi: 10.1063/1.357149.

[19] D. C. Walter, D. Bredemeier, R. Falster, V. V. Voronkov, and J. Schmidt, "Easy-to-apply methodology to measure the hydrogen concentration in boron-doped crystalline silicon," *Sol. Energy Mater. Sol. Cells*, vol. 200, Sep. 2019, Art. no. 109970, doi: 10.1016/j.solmat.2019.109970.

[20] R. A. Sinton and A. Cuevas, "Contactless determination of current–voltage characteristics and minority-carrier lifetimes in semiconductors from quasi-steady-state photoconductance data," *Appl. Phys. Lett.*, vol. 69, no. 17, pp. 2510–2512, 1996. 10.1063/1.117723.

[21] Mobility Calculator, *PV Lighthouse*, [Online]. Available: https://www2.pvlighthouse.com.au/calculators/mobility%20calculator/mobility%20calculator.aspx

[22] D. Klaassen, "A unified mobility model for device simulation - I. Model equations and concentration dependence," *Solid-State Electron.*, vol. 35, no. 7, pp. 953–959, Jul. 1992, doi: 10.1016/0038-1101(92)90325-7.

[23] D. Klaassen, "A unified mobility model for device simulation - II. Temperature dependence of carrier mobility and lifetime," *Solid-State Electron.*, vol. 35, no. 7, pp. 961–967, Jul. 1992, doi: 10.1016/0038-1101(92)90326-8.

[24] P. P. Altermatt, A. Schenk, B. Schmithüsen, and G. Heiser, "A simulation model for the density of states and for incomplete ionization in crystalline silicon. II. Investigation of Si:As and Si:B and usage in device simulation," *J. Appl. Phys.*, vol. 100, no. 11, 2006, Art. no. 113715, doi: 10.1063/1.2386935.

[25] R. Pässler, "Dispersion-related description of temperature dependencies of band gaps in semiconductors," *Phys. Rev. B*, vol. 66, no. 8, 2002, Art. no. 085201, doi: 10.1103/physrevb.66.085201.

[26] A. Schenk, "Finite-temperature full random-phase approximation model of band gap narrowing for silicon device simulation," *J. Appl. Phys.*, vol. 84, no. 7, pp. 3684–3695, 1998, doi: 10.1063/1.368545.

[27] V. V. Voronkov and R. Falster, "Formation, dissociation, and diffusion of various hydrogen dimers in silicon," *Physica Status Solidi B*, vol. 254, 2017, Art. no. 1600779, doi: 10.1002/pssb.201600779.

[28] A. Herguth and G. Hahn, "Kinetics of the boron-oxygen related defect in theory and experiment," *J. Appl. Phys.*, vol. 108, no. 11, 2010, Art. no. 114509, doi: 10.1063/1.3517155.

[29] M. Sheoran *et al.*, "Hydrogen diffusion in silicon from plasma-enhanced chemical vapor deposited silicon nitride film at high temperature," *Appl. Phys. Lett.*, vol. 92, no. 17, 2008, Art. no. 172107, doi: 10.1063/1.2917467.

[30] D. Kiliani *et al.*, "Minority charge carrier lifetime mapping of crystalline silicon wafers by time-resolved photoluminescence imaging," *J. Appl. Phys.*, vol. 110, no. 5, 2011, Art. no. 054508, doi: 10.1063/1.3630031.

[31] L. E. Black and D. H. Macdonald, "Accounting for the dependence of coil sensitivity on sample thickness and lift-off in inductively coupled photoconductance measurements," *IEEE J. Photovolt.*, vol. 9, no. 6, pp. 1563–1574, Nov. 2019, doi: 10.1109/jphotov.2019.2942484.

[32] E. Schneiderlöchner, R. Preu, R. Lüdemann, and S. W. Glunz, "Laser-fired rear contacts for crystalline silicon solar cells," *Prog. Photovolt., Res. Appl.*, vol. 10, no. 1, pp. 29–34, 2002, doi: 10.1002/pip.422.

[33] V. Naumann *et al.*, "Local electronic properties and microstructure of individual laser-fired contacts," *Proc. 24th EU-PVSEC*, 2009, pp. 2180–2184, doi: 10.4229/24thEUPVSEC2009-2DV.1.55.

[34] A. Herguth, "On the meaning(fulness) of the intensity unit 'suns' in light induced degradation experiments," *Energy Procedia*, vol. 124, pp. 53–59, 2017, doi: 10.1016/j.egypro.2017.09.339.